Single Drop Impaction on a Solid Surface

Heungsup Park and Wallace W. Carr
School of Polymer Textile and Fiber Engineering, Georgia Institute of Technology, Atlanta, GA 30332

Junyong Zhu
Institute of Paper Science and Technology, Atlanta, GA 30318

Jeffrey F. Morris
Halliburton Energy Services, Duncan, OK 73536

An experimental and theoretical study is presented on spreading and retracting of a single drop impacting on a smooth surface at room temperature. The experimental study showed the influence of kinetic energy, liquid-solid interaction, and energy dissipation on the impact process. The results are reported for Reynolds number from 180 to 5,513, Weber number from 0.2 to 176, four different liquids (distilled water, n-Octane, n-Tetradecane, and n-Hexadecane), and four different surfaces (slide glass, uncoated silicon wafer, HMDS coated silicon wafer, and Teflon film). A theoretical model based on an energy balance was developed to predict the maximum spreading ratio at low impact velocity. The key novel feature of this model is that the shape of the drop is assumed to be a spherical cap during the spreading process. When compared to models in the literature, the present model not only gives better predictions for low drop impact velocities, but also in most cases gives predictions that are within 10% of the experimental data at high impact velocities.

Introduction

The impacting and spreading of liquid drops on solid surfaces are scientifically and practically important physical processes in many applications such as spray coating, delivery of agricultural chemicals, as well as ink jet printing. The earliest work is that of Worthington (1877) who reported an investigation of drops of liquids falling vertically on a horizontal plate. Since then, there have been a number of investigations on the subject. While some of the investigations have been entirely experimental (Bergeron et al., 2000; Šikalo et al., 2002), most of the studies have included theoretical and/or numerical modeling approaches for predicting the spreading phenomenon. The theoretical approach (Engel, 1955; Ford and Furmidge, 1967; Chandra and Avedisian, 1991; Asai et al., 1993; Fukai et al., 1998) involves the use of an energy balance on the system, which consists of the drop and the impacted surface, to develop an equation for predicting the maximum spreading ratio D_m^* (ratio of the maximum spreading diameter to initial drop diameter) as a function of drop properties and contact angle. Numerical modeling (Harlow and Shannon, 1967; Fukai et al., 1993, 1995, 1998; Pasandideh-Fard et al., 1996; Bussmann et al., 1999) has been used to simulate the dynamics of transient flow and to predict the drop impacting process. These studies provide a good understanding of the effects of impacting velocity and liquid properties, that is, viscosity and surface tension, on the impacting process. However, the understanding of the solid-liquid interaction and its effects on the impacting process during spreading and recoiling is far from complete, especially its relative importance during different stages.

Several equations for predicting D_m^* based on correlations and/or energy conservation are available in the literature. One of the first correlation equations was presented by Engel (1955). Since then, there have been several efforts (Ford and Furmidge, 1967; Chandra and Avedisian, 1991; Asai et al., 1993; Pasandideh-Fard et al., 1996; Mao et al., 1997; Fukai et al., 1998) to improve the accuracy of the prediction. The earlier investigations are summarized by Mao et al. (1997) and

Correspondence concerning this article should be addressed to W. W. Carr.

Table 1. Liquid Properties and Contact Angles of Liquids on Various Surfaces

	Liquid Properties			Equilibrium Contact Angles (°)			
	Viscosity (mPas)	Density (10^3kg/m^3)*	Surface tension (mN/m)	Teflon film	HMDS coated silicon wafer	Uncoated silicon wafer	Slide glass
Distilled water	1.0	1.0	73	113	73	33	31
n-Octane	0.54	0.703	22	31	0	0	†
n-Tetradecane	2.17	0.763	26	†	0	0	†
n-Hexadecane	3.34	0.773	30	50	0	0	†

*Data from Weast (1977) *Handbook of Chemistry and Physics*, CRC Press.
†The combinations were not used.

Fukai et al. (1998). Two of the most recent predictive equations were presented by Mao et al. (1997) and Fukai et al. (1998). Their models accurately predict D_m^* for most cases except at low Reynolds and Weber numbers where they overestimate the experimental values, particularly at high and low contact angles, or may give negative or imaginary values at high contact angles.

The model by Mao et al. (1997) is based on the work of Chandra and Avedisian (1991) and Pasandideh-Fard et al. (1996), but improvements in the model were made. In the earlier work, surface-vapor and surface-liquid interaction energies during spreading were included which resulted in cos θ, where θ is the contact angle, appearing in the predictive equation. While Pasandideh-Fard et al. (1996) used the advancing contact angle in their predictions, Mao et al. (1997) used the static contact angle. Fukai et al.'s (1998) model was also based on Chandra and Avedisian's (1991) model. They improved the predictions by modifying the model to contain three empirical coefficients, which were determined by fitting them to their numerical results. We believe that the static contact angle is more appropriate since Young's Equation was used to replace the difference between interfacial energies of solid-liquid and solid-vapor, which resulted in cos θ appearing in the predictive equation.

In the present work, a comprehensive experimental study on the impaction of a single drop on several smooth surfaces was conducted to provide a foundation for conducting further study on droplet impingement on to textiles. Therefore, splashing phenomenon, which is not relevant to ink jet printing, was not included in this study. A model was developed to improve predictions of the spreading ratio at low Reynolds and Weber numbers ($Re = \rho u d/\mu$ and $We = \rho u^2 d/\gamma_{LV}$, where ρ, u, d, μ, and γ_{LV} are the liquid density, impact velocity, drop diameter, viscosity, and liquid surface tension, respectively). The model differs from previous models in that a term is added to the energy balance equation to better fit experimental values of D_m^* for low Reynolds and Weber numbers, and the drop shape at D_m^* is assumed to be a cap of a sphere instead of a cylindrical disk. As the drops used in applications such as inkjet printing are small, typically well below 100 micron dia., values of $Re = 2.5$–$2{,}000$ and $We = 2.7$–$1{,}000$ may be expected in our motivating application.

Experimental

Materials

The liquids used in the tests were distilled water, *n*-Octane, *n*-Tetradecane, and *n*-Hexadecane (Aldrich). A Brookfield Viscometer (model DV-1) was used to measure the viscosity of the fluid. A Bubble Pressure Tensiometer (BP2 Krüss GmbH) was used to measure dynamic surface tension. Four smooth surfaces were used in the tests: (1) a slide glass (Fisher Scientific), (2) an uncoated silicon wafer, (3) a silicon wafer coated with 1,1,1,3,3,3, Hexamethyl disilazane (HMDS, Aldrich) applied using a CEE Model 100CB Spinner, and (4) a Teflon coated aluminum film (Bytac Teflon Surface Protectors). The slide glass and Teflon film surfaces are highly hydrophilic and hydrophobic surfaces, respectively. Contact angles of liquids on the surfaces were measured using a VCA2500KE Contact Angle Surface Analysis System (AST Products Inc.). The surface tensions, viscosities, and densities of the liquids and the contact angles of the liquids on the various substrates are given in Table 1.

Apparatus

Two experimental setups were used for the drop impingement tests. For both setups, a syringe pump (Model 230; KD Scientific Corp., New Hope, PA) connected to a flat-tipped stainless steel needle (28G) was used to generate a single drop on demand. In the first setup as shown in Figure 1, an optical trigger consisting of a detector (OPTOLOGIC QSA157, Fairchild semiconductor) and a laser light source were used. The trigger detected a falling drop when it passed through

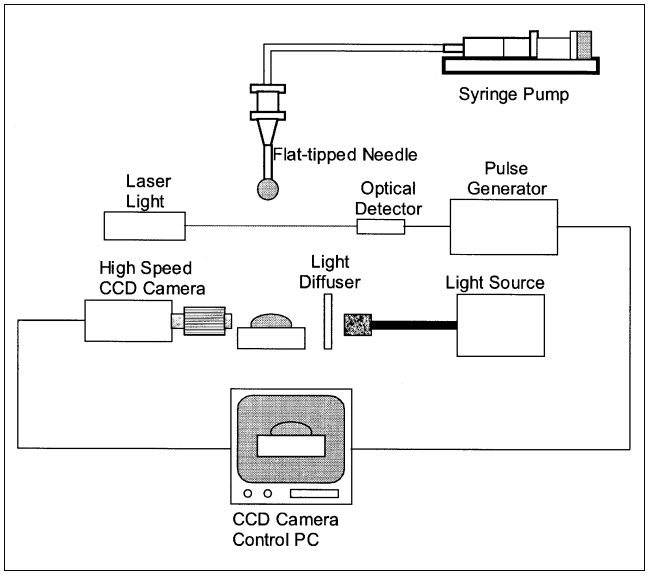

Figure 1. Experimental setup for drop impingement test using a single-drop apparatus and a SensiCam.

the laser light and sent a 5-volt TTL signal to a high-speed CCD camera (SensiCam, Cooke Corp., Auburn Hills, MI), after a preset time delay. The settings of the CCD camera were 100 μs exposure time, 800×600 pixels spatial resolution, and 8 bit gray scale in black and white. The camera captured images of the impinging drop and loaded the digital file in a computer. Replicate experiments of single drop impingement were conducted to reproduce the entire drop impingement event using different time delays of the CCD camera. The high-speed CCD camera was also used to determine drop diameter and drop speed when double exposures were superimposed in one frame.

A Kodak MotionCorder Analyzer (Eastman Kodak Company, Model 1000, San Diego, CA) was used to take continuous pictures of a single event. A series of pictures were recorded from one drop impingement event using a camera recording speed of 3,000 fps. Other settings of the camera were 200 μs exposure time, 128×96 pixels spatial resolution, and 8 bit gray scale in black and white. Drop impaction speed was calculated using droplet displacement, which was measured between two different frames using a calibrated scale, and time between frames.

The Kodak camera system was used to obtain most of the experimental data presented in the body of the article. The Kodak camera system had several advantages over the Sensicam camera system. One was obtaining data was much faster since repeated tests required by the Sensicam camera system were not necessary. This also meant fewer surfaces had to be prepared. Another was that the Sensicam camera system could not be used for the impingement test at low *Re* because the distance between the needle and the solid surface was too small to accommodate the laser triggering system. The Sensicam camera system was used for the spontaneous spreading tests because the fluid layer resulting from spontaneous spreading was very thin. The higher resolution associated with the Sensicam camera system facilitated measurement of the spreading ratio.

Models for Predicting Maximum Spreading

Models for predicting maximum drop spreading ratio ($D_m^* = D_m/d$) are discussed in this section. Previous models (Engel, 1955; Ford and Furmidge, 1967; Chandra and Avedisian, 1991; Asai et al., 1993; Pasandideh-Fard et al., 1996; Mao et al., 1997; Fukai et al., 1998) are based on an energy conservation equation, where system energy at impact (state 1) is set equal to system energy at maximum spreading (state 2). The assumptions are made that the drop volume is conserved and the drop spreads into a cylindrical disk of diameter D and height h. The cylindrical-disk assumption is reasonable except for low impact velocities, particularly for high contact angles where the surface area of the cylindrical disk is much higher than the actual surface area. In our model, we make the relatively simple change of assuming that the shape of the fluid in state 2 is a cap of a sphere rather than a cylindrical disk, again holding the fluid volume constant. This geometry which more closely represents the physics of low velocity impact leads to better predictions at low impact velocities, while giving predictions very similar to those of Mao et al. (1997) and Fukai et al. (1998) at higher Reynolds and Weber numbers.

The energy conservation equation used for previous models is

$$E_{K1} + E_{SL1} + E_{SS1} = E_{K2} + E_{SL2} + E_{Si2} + E_{V2} \qquad (1)$$

where states 1 and 2 represent impact and maximum spread, respectively. On the lefthand side of the relationship, E_{K1} is drop kinetic energy, E_{SL1} is the surface energy of the liquid, and E_{SS1} is the surface energy of the solid area at impact that will be covered with liquid at maximum spreading. On the righthand side, E_{K2} is the kinetic energy (which is zero), E_{SL2} is the surface energy of the liquid drop, E_{Si2} is the interfacial energy between the liquid drop and the solid, and E_{V2} is the energy viscously dissipated in the droplet as it is deformed from state 1 to state 2.

Equation 1 is the relationship used by several investigators (Engel, 1955; Ford and Furmidge, 1967; Chandra and Avedisian, 1991; Asai et al., 1993; Pasandideh-Fard et al., 1996; Mao et al., 1997; Fukai et al., 1998) to develop equations for predicting D_m^*. When the impact velocity is zero, Eq. 1 indicates that the surface and interfacial energies for states 1 and 2 are identical since the kinetic energies of states 1 and 2 are zero, and viscous dissipation is zero according to the relationships used to estimate E_{V2} when impact velocity is zero.

Thus, Eq. 1 becomes

$$E_{SL1} + E_{SS1} = E_{SL2} + E_{Si2} \qquad (2)$$

Equation 2 is incorrect since the drop will spontaneously spread for contact angles less than 180°, and energy will be dissipated. The failure of the energy balance is partly due to the failure of the viscous dissipation equations at low *Re*. However, even if equations were capable of predicting viscous dissipation at very low impact velocity, energy dissipated due to the heat of wetting (due to the attachment of liquid molecules to the solid) would not be accounted for. Regardless of the dissipation mechanism, the decrease in surface and interfacial energies for spontaneous spreading from state 1 to state 2 can be accounted for as described below.

It should be noted that previous models predict spreading for zero impact velocity even though the energy balance equation indicates no energy is dissipated during spontaneous spreading. This occurs because, for constant volume, the surface area of a cylindrical disk is greater than that of a spherical cap. However, the predictions are inaccurate for low and high contact angle, and sometimes negative and imaginary values of D_m^* are obtained.

Ford and Furmidge (1967) pointed out that, when a small drop is placed on a solid surface, it takes the form of a spherical cap and that D_θ^* (spreading ratio at equilibrium contact angle, θ) is given by the expression

$$D_\theta^* = \sqrt{g(\theta)} = \left[\frac{4\sin^3\theta}{2-3\cos\theta+\cos^3\theta}\right]^{1/3} \qquad (3)$$

and this suggests our approach of using a cap of a variable-radius sphere to represent the spreading drop at low impact velocities (small *Re* and small *We*). Kim and Chun (2001) have used a truncated sphere assumption in their approximate

model which utilizes the variational principle rather than the Navier-Stokes equation to predict spreading and recoiling of droplets; however, they do not present a predictive equation for D_m^*.

The decrease in surface and interfacial energies for spontaneous spreading from state 1 to state 2, $-\Delta E_{SP}$, can be calculated using the assumptions that the shape of the fluid in state 2 is a cap of a sphere and that the fluid volume is constant. The equation for ΔE_{SP} in terms of the equilibrium contact angle θ for the liquid with the solid is

$$\Delta E_{SP} = \pi d^2 \gamma_{LV} \left(\frac{\cos\theta}{4} g(\theta) - \frac{1}{2} \left(\frac{1-\cos\theta}{\sin^2\theta} \right) g(\theta) \right) \quad (4)$$

where d is impinging the drop diameter, and γ_{LV} is the surface energy of liquid-vapor.

When the energy spontaneously dissipated into heat is accounted for using ΔE_{SP}, Eq. 2 becomes

$$E_{SL1} + E_{SS1} = E_{SL2} + E_{Si2} + \Delta E_{SP} \quad (5)$$

If we assume that this amount of energy will be spontaneously dissipated into heat when the impact velocity is greater than zero, Eq. 1 becomes

$$E_{K1} + E_{SL1} + E_{SS1} = E_{K2} + E_{SL2} + E_{Si2} + E_{V2} + \Delta E_{SP} \quad (6)$$

The terms on the lefthand side of Eq. 6 can be expressed as follows

$$E_{K1} = \frac{\pi}{12} \rho d^3 u^2 \quad (7)$$

$$E_{SL1} = \pi d^2 \gamma_{LV} \quad (8)$$

$$E_{SS1} = \frac{\pi}{4} D_m^2 \gamma_{SV} \quad (9)$$

where ρ is the density of liquid drop, u is the impact speed, D_m is spreading the drop diameter at maximum, and γ_{SV} is the surface energy of solid-vapor.

Expressions for the terms on the righthand side of Eq. 6 and assumptions in writing these expressions are discussed next. The drop shape at maximum spreading was assumed to be a spherical cap, as shown in Figure 2. With this assumption, E_{SL2} can be written as

$$E_{SL2} = \frac{1}{2}\pi(1-\cos\alpha)\left(\frac{4}{2-3\cos\alpha+\cos^3\alpha} \right)^{2/3} d^2 \gamma_{LV}$$

$$= \frac{1}{2}\pi \frac{(1-\cos\alpha)}{\sin^2\alpha} g(\alpha) d^2 \gamma_{LV} \quad (10)$$

where α is the contact angle at maximum spreading calculated using the assumptions that the shape of the fluid in state 2 is a cap of a sphere and that the fluid volume is constant. The function $g(\alpha)$ (see Eq. 3) is

$$g(\alpha) = (D_m^*)^2 = \left[\frac{4\sin^3\alpha}{2-3\cos\alpha+\cos^3\alpha} \right]^{2/3} \quad (11)$$

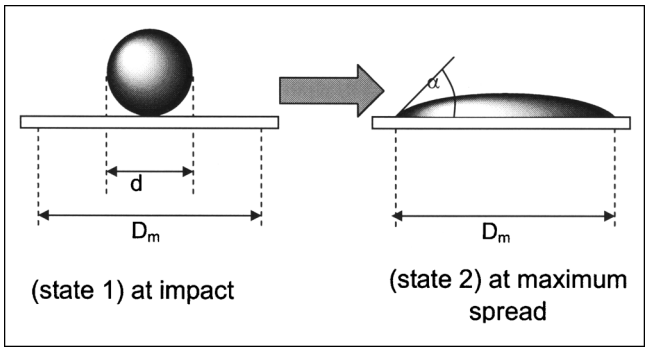

Figure 2. (State 1) at impact and (state 2) at maximum spread.

and E_{Si2} is given by

$$E_{Si2} = \frac{\pi}{4} D_m^2 \gamma_{SL} \quad (12)$$

The energy viscously dissipated in the drop E_{V2}, as it is deformed from states 1 to 2 has been treated by several investigators (Engel, 1955; Ford and Furmidge, 1967; Chandra and Avedisian, 1991; Asai et al., 1993; Pasandideh-Fard et al., 1996; Mao et al., 1997; Fukai et al., 1998). For high viscosity liquids ($Re < 81(D_m/d)^4$), E_{V2} was estimated using the following relationship, suggested by Chandra and Avedisian (1991) and Mao et al. (1997).

$$\int_0^{t_c}\int_\Omega \phi d\Omega dt \approx \phi\Omega t_c \approx 0.53 \frac{\pi\mu u D_m^4}{d^2} \quad (13)$$

For low viscosity liquids ($Re > 81(D_m/d)^4$), E_{V2} was estimated using the following relationship, suggested by Pasandideh-Fard et al. (1996) and Mao et al. (1997)

$$\int_0^{t_c}\int_\Omega \phi d\Omega dt \approx \phi\Omega t_c \approx \mu \left(\frac{\partial^2 u}{\partial y^2} \right) \left(\frac{1}{4}\pi D_m^2 \delta \right) \left(\frac{8}{3}\frac{d}{u} \right)$$

$$= 0.33\pi \frac{\rho u^2 d}{\sqrt{Re}} D_m^2 \quad (14)$$

Substituting these relations into Eq. 1, using Young's equation and the definitions of $Re = \rho u d/\mu$ and $We = \rho u^2 d/\gamma_{LV}$, setting $D_m^* = D_m/d$, and rearranging gives the following two relationships. The first is for high viscosity liquids such as glycerin, and the second is for low viscosity liquids such as water

$$0.53\frac{We}{Re} D_m^{*4} + \left(\frac{1}{2}\left(\frac{1-\cos\alpha}{\sin^2\alpha} \right) - \frac{1}{4}\cos\theta \right) D_m^{*2}$$

$$-1 - \frac{We}{12} + \frac{\Delta E_{SP}}{\pi d^2 \gamma_{LV}} = 0 \quad (15a)$$

$$\left(0.33\frac{We}{\sqrt{Re}} - \frac{1}{4}\cos\theta + \frac{1}{2}\left(\frac{1-\cos\alpha}{\sin^2\alpha}\right)\right)D_m^{*2}$$

$$-1 - \frac{We}{12} + \frac{\Delta E_{SP}}{\pi d^2 \gamma_{LV}} = 0 \quad (15b)$$

These equations can be solved simultaneously with Eq. 11 to obtain D_m^*. (Note that ΔE_{SP} is calculated using Eq. 4.)

Results and Discussion

Effect of substrate on stages of the impact process

The stages of the impact process observed in our experimental studies are discussed first. These stages depend on the liquid and the interaction of the liquid with the substrate. The parameter used to characterize the impact process will be the drop spreading ratio ($D^* = D/d$), the diameter of the liquid-solid interface to the initial diameter of the impacting drop.

Figure 3 illustrates the impacting process measured using the high speed (Kodak) camera to record the impaction process from drop impact to final resting position in one experiment. The figure shows the spreading ratio of a 2.3 mm water drop with impact speed of 1 m/s on various surfaces at room temperature. The *Re* and *We* at this impact velocity and diameter are 2,000 and 24, respectively.

During the spreading stage (B), similar values of D^* are observed for the four substrates. The images taken at state 1, t (time) = 0.0 ms, show the spherically shaped drops just before impact. At state 2, the drops on the various surfaces were approximately at the maximum spreading ratio (D_m^*), which occurred at $t \approx 1.7$ ms for the drops on the HMDS coated silicon wafer and the Teflon film and at $t \approx 2.0$ ms for the drops on the slide glass and uncoated silicon wafer surfaces. The maximum spreading ratios on the slide glass and the silicon wafer are only about 10–20% greater than that on other surfaces. This is related to the surface energies of the slide glass and the silicon wafer being higher and the contact angles for water on these surfaces being lower (see Table 1).

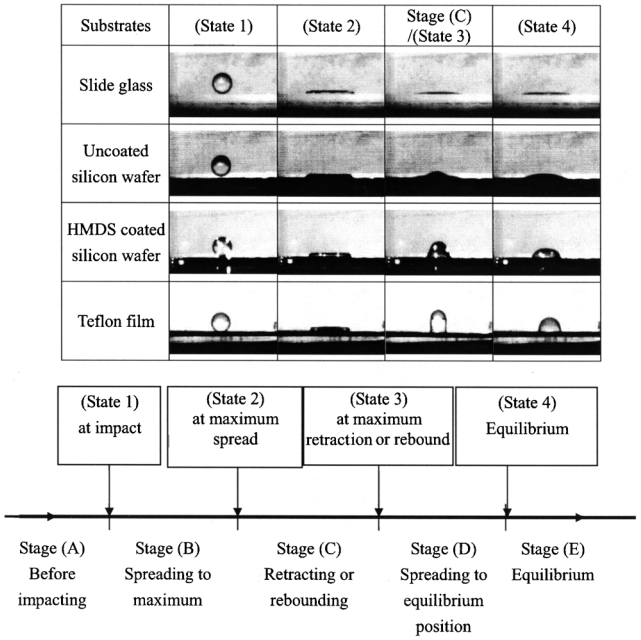

Figure 3. Spreading and retracting of a 2.3 mm water drop impacting horizontal smooth surfaces at 1 m/s (spreading coefficient < 0).

In the retracting/rebounding stage (C), the liquid retracts much further for drops on the HMDS coated silicon wafer and the Teflon film, which are hydrophobic surfaces. In fact for the slide glass and uncoated silicon wafer, which are hydrophilic surfaces, the liquid retracts to the final spreading ratio, with no discernible retraction beyond the equilibrium spreading position. On the other hand, retraction for the hydrophobic surfaces goes far beyond the equilibrium spreading position. At state 3, $t \approx 4.5$ ms, the drops on the Teflon film and polymer coated silicon wafer rise up, but do not leave the surface for an impact speed of 1 m/s. At an impact speed of about 2.36 m/s, the drop on the Teflon film rose slightly above the surface. However, even at this impact speed, the drops on the hydrophilic surfaces retract to the final spreading ratio with no discernible retraction beyond the equilibrium spreading position.

After maximum retraction, D^* increases until the equilibrium spreading ratio is reached at state 4, $t \approx 10.0$ ms. The resting spreading ratios for the four surfaces correlate with the static contact angles for water on these substrates. They are close to the values obtained when a droplet is placed on the surfaces with approximately zero impact velocity.

Effect of drop kinetic energy

Figure 4 shows the influence of impacting kinetic energy (velocity) on the spreading and retracting processes for a water drop impacting on various surfaces. Our experiments were performed using water drops having impact velocities from about 0.08 to 2.36 m/s, and a diameter of 2.3 mm, conditions which correspond to Reynolds numbers from about 180 to 6,000. The maximum spreading ratio increases with increasing impact velocity for all of the surfaces as expected (Ford and Furmidge, 1967; Cheng, 1977; Scheller and Bousfield, 1995; Šikalo et al., 2002). Figure 4a is for water on a hydrophilic surface (slide glass), and Figure 4b is for water on a hydrophobic surface (Teflon film). As discussed above, the impacting process for the hydrophilic surface has only two stages: spreading to the maximum spreading ratio and retracting to the equilibrium spreading ratio. The impacting process for the hydrophobic surface includes spreading, retracting and sometimes rebounding if impact velocity is high enough, and then spreading to the equilibrium spreading ratio. The final equilibrium spreading ratio is primarily determined by the solid-liquid interaction and varies slightly with impacting velocity.

Pasandideh-Fard et al. (1996) estimated dimensionless time ($t^* = t \cdot u/d$) to reach a maximum spreading ratio to be a constant of 8/3. In the expression for t^*, t is time, u is impact velocity, and d is drop diameter. However, it was found that t^* increases from 0.32 to 3.08 as the impact velocity increases from 0.08 to 2.36.

When the impact velocity approaches zero, the impact process is dominated by the interaction of the liquid and solid surface. This is illustrated in Figure 5 for a 2.3 mm diameter

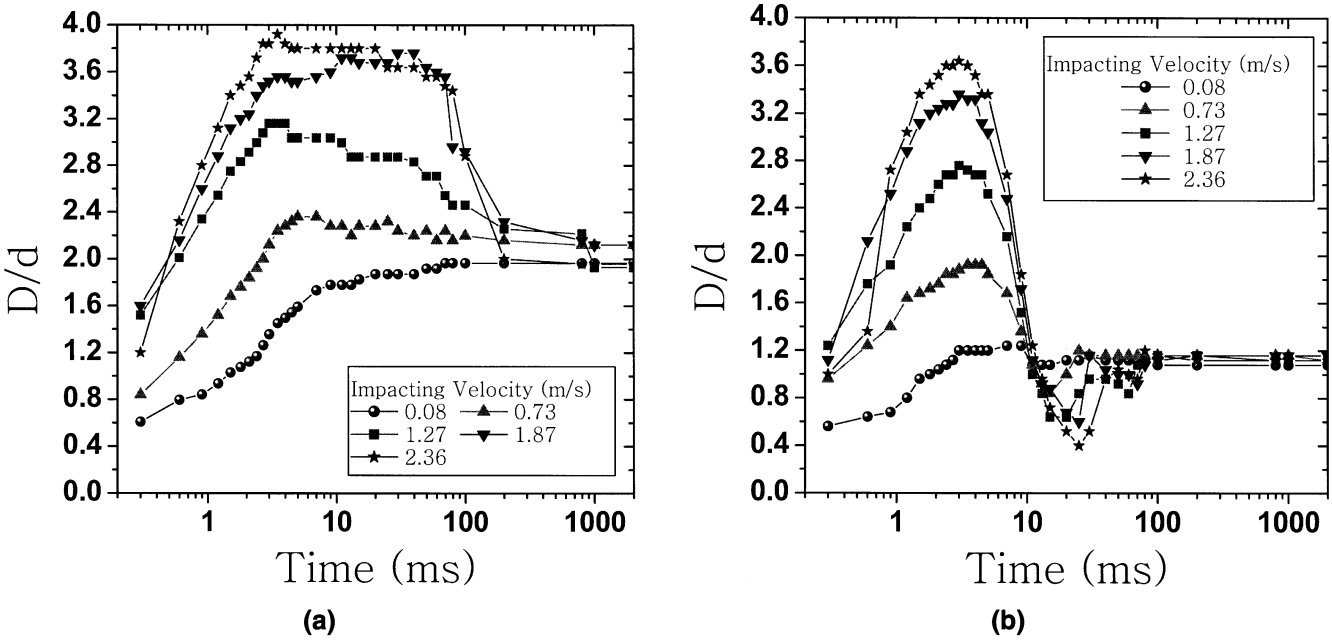

Figure 4. Spreading and retracting of a 2.3 mm water drop on two surfaces: (a) Slide glass ($\theta = 31°$) and (b) Teflon film ($\theta = 113°$).

water drop at an impact velocity of 0.08 m/s. After reaching the maximum spreading ratio (which is close to the equilibrium spreading ratio), a small amount of retracting and spreading may be present, but it is too small to be detected by the Kodak camera system used for this test.

Influence of solid-liquid interactions

The impact process is greatly affected by the solid-liquid interaction, which can be characterized using a parameter called the "normalized spreading coefficient." When a unit area of solid-vapor interface is replaced with a unit area of liquid-solid interface and a unit area of liquid-vapor interface (liquid surface area is increased during spreading), the change of Gibbs free energy (per unit area) is given by the following expressions (de Gennes, 1985; Hiemenz and Rajagopalan, 1997)

$$\Delta G = -S = \gamma_{LS} + \gamma_{LV} - \gamma_{SV} \tag{16}$$

where S is the spreading coefficient, γ_{LS} is interfacial energy between liquid and solid, γ_{LV} is surface energy of liquid with vapor, and γ_{SV} is surface energy of solid with dry air (vapor). The normalized spreading coefficient is obtained by dividing through by γ_{LV}

$$\frac{S}{\gamma_{LV}} = \frac{\gamma_{SV} - \gamma_{LS}}{\gamma_{LV}} - 1 \tag{17}$$

For a static contact angle $\theta > 0$, Eq. 17 can be combined with Young's equation to give

$$\frac{S}{\gamma_{LV}} = \cos\theta - 1 \tag{18}$$

Figure 6 shows the effect of a normalized spreading coefficient, S/γ_{LV}, on D_m^* of a water drop of dia. 2.3 mm with various impact velocities, for S/γ_{LV} ranging from -1.39–-0.14. We have not shown data for $S/\gamma_{LV} \geq 0$ because this corresponds to spontaneous spreading to very large values of D_m^* which will be discussed later. Our data agree well with those reported by Mao et al. (1997). The maximum spreading ratio increases with increasing S/γ_{LV}, for all impacting velocity, but the effect of solid-liquid interactions on the maximum spreading diameter is more pronounced at low impacting velocities. At an impact velocity of 0.086 m/s, drop spreading is

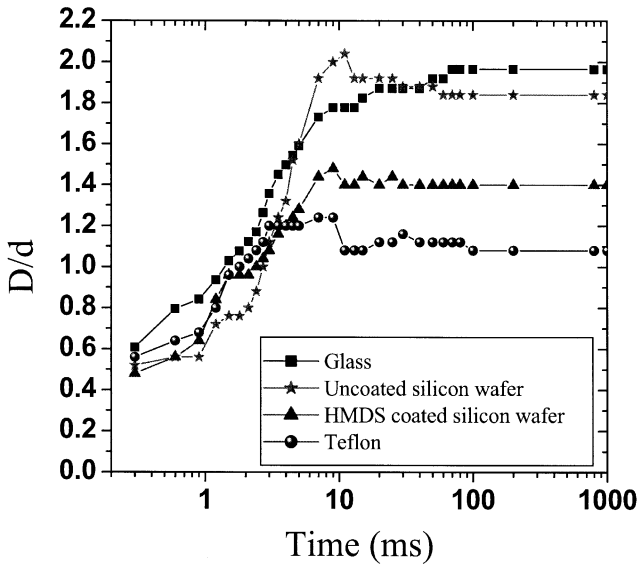

Figure 5. Spreading of a 2.3 mm water drop on various surfaces at a very low impact velocity of 0.08 m/s.

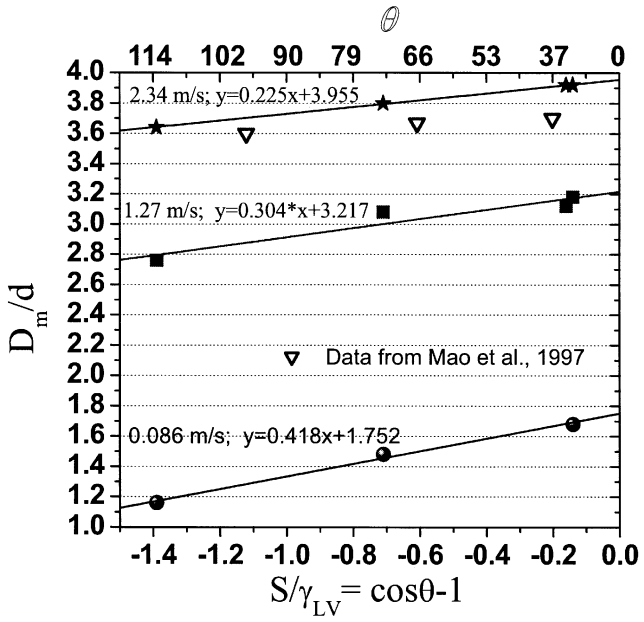

Figure 6. Effect of normalized spreading coefficient on maximum spreading ratio of water drop impacting various surfaces.

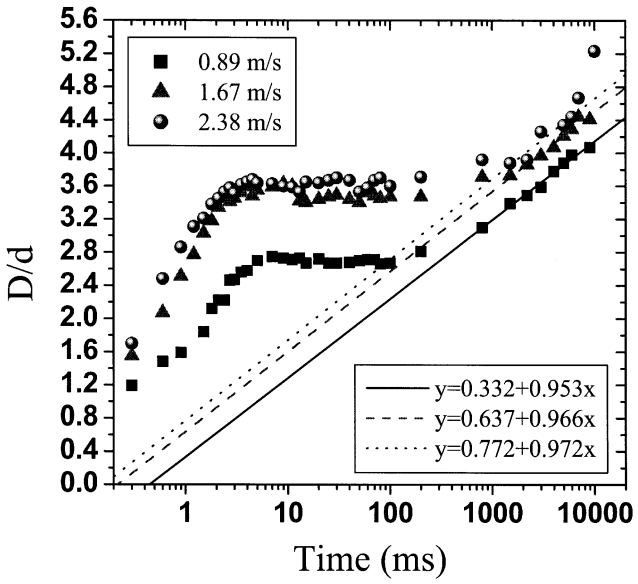

Figure 7. Effect of impact velocity on spread ratio for a liquid that spontaneously spreads over surface—a 2.0 mm *n*-Tetradecane drop on an uncoated silicon wafer surface.

primarily driven by solid-liquid interactions. For the surface where S/γ_{LV} is about -0.14, the D_m/d is about 45% greater than for the surface where S/γ_{LV} is about -1.39. At an impact velocity of 2.34 m/s, D_m^* increased by only 8% when S/γ_{LV} increased from -0.14–-1.39. Note that the kinetic energy of the drop was increased by almost 800 times when the drop velocity increased from 0.08 to 2.34 m/s. Furthermore, at impacting velocity of 2.34 m/s, the kinetic energy of the impacting drop is about 14.7 times larger than the impacting drop surface energy. Therefore, kinetic energy dominates the impacting and spreading process.

Spreading coefficient greater than and equal to zero

When the spreading coefficient is greater than zero, liquid will spontaneously spread over the surface as shown in Figure 7 for a 2 mm drop of *n*-Tetradecane on uncoated silicon. For zero impact velocity, the variation of D^* with time is well fitted by a power-law relationship (Marmur, 1988; Lin et al., 1996). For impact velocity greater than zero, there is an initial period where the spreading is driven by the kinetic energy of the impacting drop, and D^* increases much faster than that for the zero impact velocity case. After the initial rapid spreading period, D^* is almost constant for a period of time. Spontaneous spreading then begins, and the variation of D^* with time is well fitted by a power-law relationship as shown. Linear regression of the data indicates that the exponential index increase slightly with the increase of impacting velocity as shown.

Energy dissipation

Kinetic and surface energies are dissipated during an impact process, but mechanisms for the dissipation processes are not completely understood. de Gennes (1985) discussed several types of dissipative processes that can occur during spreading of a liquid. These processes can occur in the following three locations: (1) the wedge of fluid behind the contact line, (2) the extremely thin (submicron thickness) precursor film which shows up ahead of the nominal contact line, and (3) the region in the close vicinity of the real contact line. Therefore, energy dissipation includes both viscous dissipation in the bulk fluid and dissipation in the vicinity of the contact line. According to the theory discussed by Blake and De Coninck (2002), solid-liquid interactions are a major source of energy dissipation within the moving three-phase zone.

The influence of viscous dissipation on the impacting process is illustrated in Figure 8, where D^* vs. time for two types of alkane drops of 2 mm dia. and 1.9 m/s impact velocity on a Teflon film surface is shown. Weber numbers are almost the same (158 for *n*-Octane and 160 for *n*-Hexadecane), and, thus, the ratios of inertial to surface energies are almost the same for the two cases. On the other hand, since the viscosity of the *n*-Hexadecane is about 6.2 times greater than for *n*-Octane, Reynolds numbers are quite different (4,087 for *n*-Octane and 856 for *n*-Hexadecane). Thus, the viscous effects relative to inertial effects are about 4.8 times greater for the *n*-Hexadecane. The spreading ratio was nearly the same during the early stages of spreading ($t < 1$ ms, $t^* \approx 0.85$). However, the maximum spreading ratio is lower for the *n*-Hexadecane drop (about 77% of that of the *n*-Octane drop) because viscous dissipation in the *n*-Hexadecane is much higher.

Both liquids retract to the resting position in about the same time, although the *n*-Octane drop has further distance to retract. There is no discernible retraction beyond the resting position for either liquid. The final resting spreading ratio of the *n*-Hexadecane drop is smaller than that of the *n*-Octane, which is due to the surface-liquid interactions (equi-

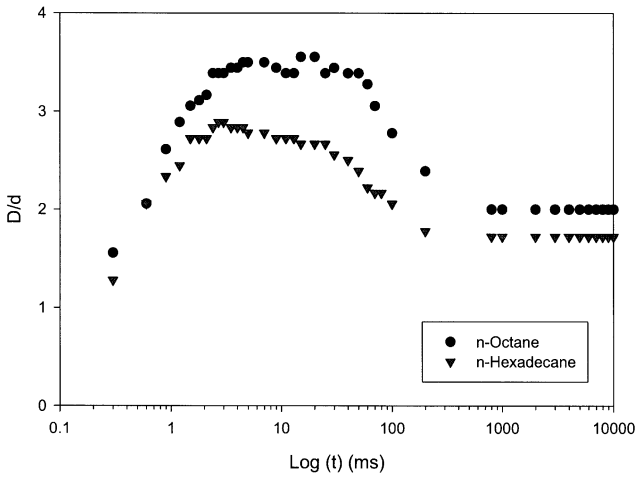

Figure 8. Spreading of 2 mm alkane drops with impact velocity of drop, 1.9 m/s, on a Teflon film surface.

Re of 4087 (*n*-Octane) and 856 (*n*-Hexadecane), and *We* of 158 (*n*-Octane) and 160 (*n*-Hexadecane).

librium contact angle of *n*-Hexadecane is about 50°, while it is about 31°). These observations on the effect of viscosity on the maximum spreading ratio and final resting spreading ratio agree qualitatively with those reported by Scheller and Bousfield (1995).

The effect of solid-liquid interaction on the retraction of the drop from maximum spreading is illustrated in Figure 9. Spreading ratios of 2.3 mm water drops impacting four different smooth surfaces at $u = 1.27$ m/s are shown. Since the impact velocity and drop diameter are held constant, the Reynolds and Weber numbers are almost identical for the four experiments, that is, 3,003 and 53, respectively. Thus, the major difference is the solid-liquid interaction, which is characterized by $\cos\theta$, where θ is the static contact angle. Kinetic energy of the impacting drop and viscous energy dissipation dominate during initial spreading in the impacting stage, and the spreading ratio is almost identical until the maximum spreading ratio is approached. The maximum spreading ratio is slightly higher for the slide glass, as expected, due to strong solid-liquid interaction (the spreading coefficient is highest) for water on the slide glass.

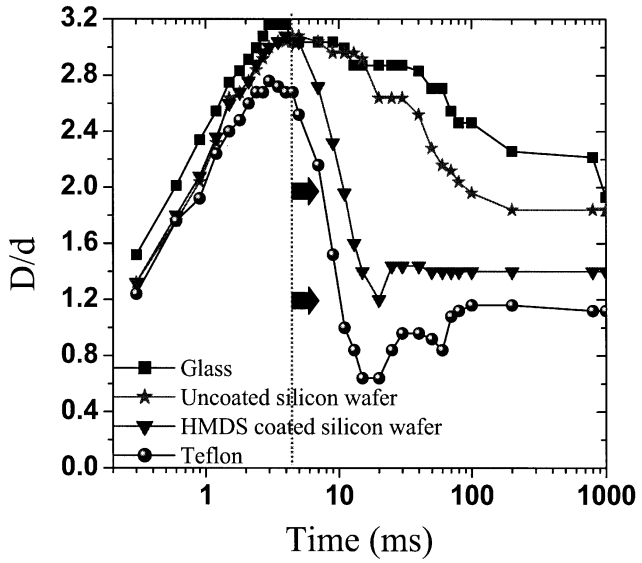

Figure 9. Effect of liquid-surface interaction on the retracting (Stage C) of a 2.3 mm water drop impacting the surfaces at 1.27 m/s.

Re = 3,003; *We* = 53.

At maximum spreading ratio, the surface energy stored in the liquid-vapor interface is greater than for the equilibrium drop shape. As a result, the contact angle decreases below its equilibrium value, and D^* decreases. Although water is used for all four experiments, its spreading behavior on the four surfaces is quite different. The drop retracts much more slowly on the slide glass and uncoated silicon wafer and does not retract as far. The drops on the HMDS coated silicon wafer and Teflon film not only retract much faster, but retract through the equilibrium position, and then spread back to the equilibrium position. Because viscosity is the same in the four experiments, the difference in the behavior after the drop reaches the maximum spreading ratio must be explained by some other factor.

The amount of retraction depends on the strength of the liquid-surface interaction since (assuming there is not a microscopic film that we cannot detect by our experimental method) retraction requires liquid to be removed from the solid surface. The energy required to remove the liquid from the surface is related to the work of adhesion W_{ab}. As the drop retracts, excess surface energy stored in the liquid-vapor surface is consumed in three ways: (1) used to remove liquid from the solid surface, (2) converted into kinetic energy in the liquid, and (3) viscously dissipated. As W_{ab} is increased, less energy is available to be converted into kinetic energy and viscous dissipation, and, thus, retraction decreases.

The work of adhesion W_{ab} is the work necessary to separate a unit area of a solid-liquid interface into a unit area of a solid-vapor interface and a unit area of liquid-vapor interface. W_{ab} is equal to the net change of Gibbs free energy per unit area

$$\Delta G = W_{ab} = \gamma_{LV} + \gamma_{SV} - \gamma_{LS} \tag{19}$$

Using Young's equation and dividing by γ_{LV} gives the normalized work of adhesion W_{ab}/γ_{LV}

$$\frac{W_{ab}}{\gamma_{LV}} = 1 + \cos\theta \tag{20}$$

The relationship between the minimum spreading ratio $D^*_{\min}$, during retraction and W_{ab}/γ_{LV} is shown in Figure 10 for water drops having a dia. of 2.3 mm at a varying speed of impact. Retraction is much lower for the two cases where W_{ab}/γ_{LV} is large and does not change much with impact velocity. As W_{ab}/γ_{LV} decreases, $D^*_{\min}$ is reduced since less excess surface energy in the liquid-vapor surface is consumed in removing liquid from the solid surface. For the lower values of W_{ab}/γ_{LV}, the drop retracts through the equilibrium posi-

Table 2. Experimental Results Compared with Model Predictions for Low Impact Velocity

	Impact velocity (m/s)	Equilibrium Contact Angle (°)	Experimental data	Mao et al.'s (1997) model	Fukai et al.'s (1998) model	Present model[#]
$We = 0.2$*	0.082	113	1.16	[‡]	1.13	1.16
$Re = 180$		73	1.48	1.9213	1.58	1.55
		33	1.68	4.9204	3.52	2.03
$We = 7$*	0.73	113	1.92	1.6484	1.4053	1.84
$Re = 1712$		73	2.08	2.2068	1.9515	2.24
		33	2.28	3.3046	3.5292	2.93
$We = 5.5$[†]	[§]	65	1.42	1.73	1.84	1.37
$Re = 58.7$						

*Data from present research.
[†]Data from Asai et al. (1993). Equilibrium contact angle of ink on a transparent film was assumed to be 65°.
[‡]Mao et al. (1997) model gives negative and imaginary prediction.
[§]Exact values not given by Asai et al. (1993), but impact velocity ranged from 2.5 to 20 m/s.
[#]Equations 11 and 15a.

tion. As impact velocity is increased, the maximum spreading ratio increases and the excess surface energy stored in the liquid-vapor surface increases. As a result, $D^*_{\min}$ decreases for cases where W_{ab}/γ_{LV} is smaller.

Maximum spreading model for strong solid-liquid interaction

In Table 2 and Figures 11 and 12, experimental values of D^*_m for a liquid drop having low impact velocity, low viscosity, and high surface tension are compared with predictions from our model and the models of Mao et al. (1997) and Fukai et al. (1998). These models were selected for comparison because they are the two best models based on the energy balance equation for accurately predicting D^*_m for most cases. At *Re* and *We* of 180 and 0.2, our model gives better predictions. For a contact angle of 33°, Mao et al.'s and Fukai et al.'s models overestimate the experimental value by 200% and 110%, respectively, while our model overestimates D^* by 21%. The model of Mao et al. (1997) gives imaginary values of D^* for $\theta > 110°$ (see Figure 11). For a contact angle of 180°, spreading at the extremely low impact velocity (0.08 m/s) is expected to be close to zero. The prediction of our model is close to zero, while the prediction of the model of Fukai et al. (1998) is approximately 1.0, which results from their assumption of a cylindrical disk shape drop. At *Re* and *We* of 1,712 and 7, our model gives better predictions of D^*_m at the low contact angle (33°) and high contact angle (113°).

In Table 2, experimental results of Asai et al. (1993) for ink jet printing at low *Re* and *We* of 58.7 and 5.5, respectively, are compared with model predictions. Our model prediction is 4% lower than the experimental value, while the models of Mao et al. (1997) and Fukai et al. (1998) predict values that are 22 and 30% greater than the experimental value, respectively.

In Figure 13, model predictions are compared with experimental values of D^*_m for higher impact velocity (*Re* and *We* of 5,513 and 176, respectively) where kinetic energy domi-

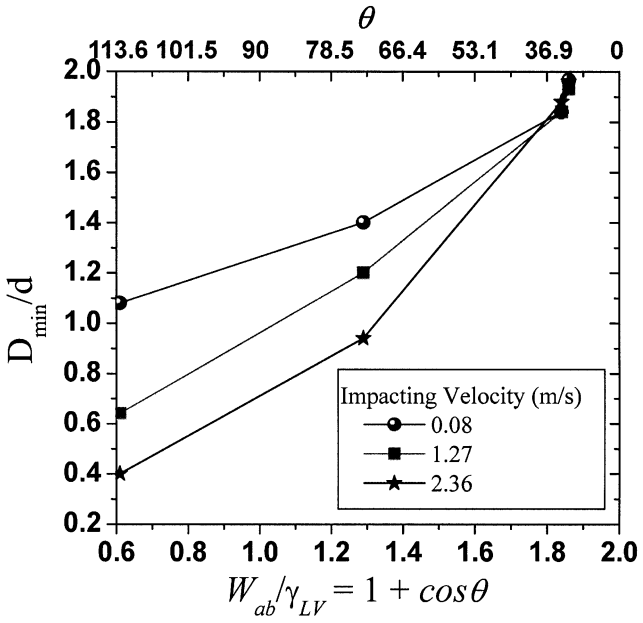

Figure 10. Effect of normalized work of adhesion on minimum value of spreading ratio during retraction of a water drop.

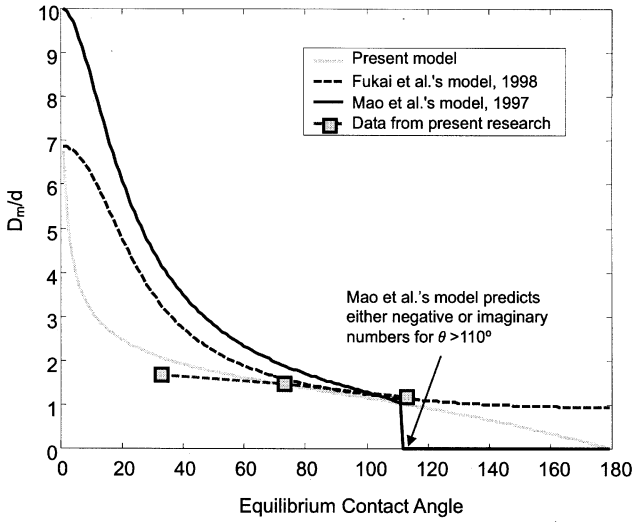

Figure 11. Maximum spreading ratio predicted by several models at *Re* = 180 and *We* = 0.2.

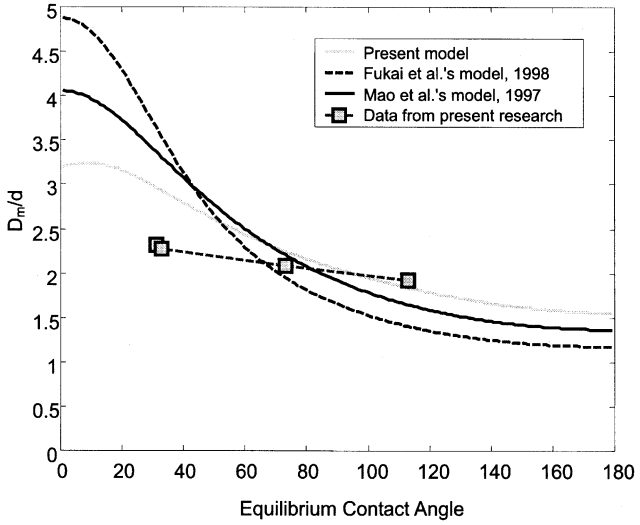

Figure 12. Maximum spreading ratio predicted by several models at *Re* = 1,712 and *We* = 7.

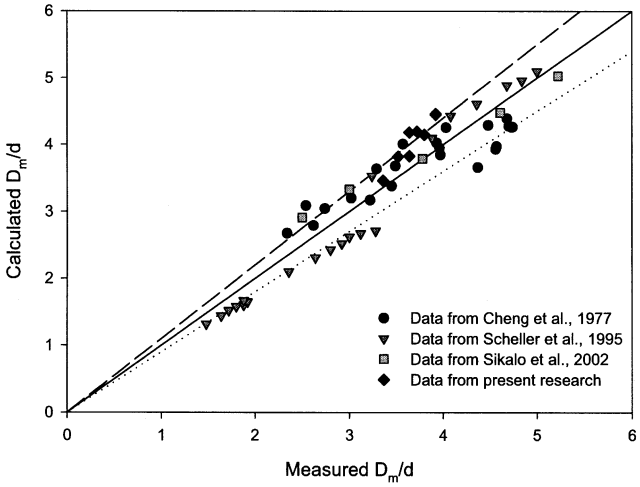

Figure 14. Comparison of current model predictions with experimental results reported in the literature.

The solid line is the model value, and the lines above and below represent ten percent deviation level.

nates. All three models predict the experimental results fairly well except at the contact angle of 33°, where the model of Fukai et al. (1998) overpredicts by about 21%.

The data from the present research and literature are compared with our model predictions in Figure 14. The experimental results are for impact studies for $18 < Re < 12{,}958$, $32 < We < 2{,}277$ and $35 < \theta < 100$. Equation 15a was used for the predictions in all cases except for data from Scheller and Bousfield (1995), where viscosity was high (300 mPa·s). For these data, Eq. 15b was used. The predictions of present models are within 10% of most of the experimental data.

Conclusion

The stages of the impact process of a drop on a smooth surface depend on the interaction of the liquid with the surface. Considered for water, the impact process for the hydrophilic surface has only two stages: spreading to the maximum spreading ratio D_m^*, and retracting to the equilibrium spreading ratio. The impact process for the hydrophobic surface includes: spreading, retracting, and sometimes rebounding if impact velocity is high enough, and then spreading to the equilibrium spreading ratio. The final equilibrium spreading ratio is primarily determined by the solid-liquid interaction and varies slightly with impacting velocity.

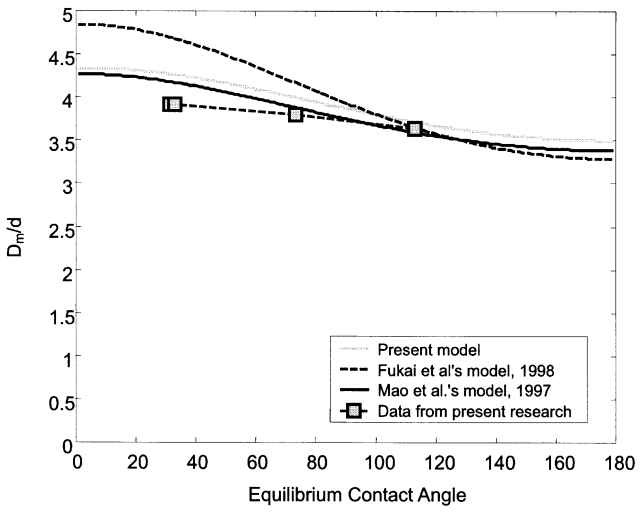

Figure 13. Maximum spreading ratio predicted by several models at *Re* = 5,513 and *We* = 176.

At low impact velocity, D_m^* is primarily determined by solid-liquid interaction. D_m^* for a water drop on the hydrophilic surfaces is greater than for the hydrophobic surfaces. As impact velocity (kinetic energy) is increased, D_m^* increases. At high impact velocity, D_m^* is primarily determined by kinetic energy and was only about 10–20% greater for the hydrophobic surfaces. Increasing the viscosity of the impacting drop (which results in a reduction in the Reynolds number if all other parameters are held constant) increases the rate of viscous dissipation and reduces D_m^*. It also decreases the rate of retraction from D_m^*.

When the spreading coefficient is greater than zero, liquid spontaneously spreads over the surface. For an impacting drop, there is an initial period where the spreading is driven by the kinetic energy. After the initial rapid spreading period, D^* is almost constant for a period of time. Then, spontaneous spreading begins, and the variation of D^* with time is well fitted by a power-law relationship.

At D_m^*, excess surface energy stored in the liquid-vapor surface causes retraction. The amount of retraction depends on the strength of the liquid-surface interaction since retraction requires liquid to be removed from the solid surface. The energy required to remove the liquid from the surface can be related to the work of adhesion W_{ab}. The rate and amount of retraction decrease with increasing W_{ab}.

A theoretical model based on an energy balance was developed to predict the maximum spreading ratio at low impact velocity. The main new feature of the model lies in the simple geometrical assumption of a spherical cap, rather than a

cylindrical disk as in most prior work, for the spreading drop. This geometrical assumption, designed to provide better small-*Re* and small-*We* predictions, leads to predictions which when compared to existing models in the literature are not only better for low drop impact velocities (small *Re* and *We*), but in most cases are within 10% of the experimental data even at high impact velocities.

Acknowledgments

This work was supported by the National Textile Center (C99-GT07 and (C02-GT08).

Literature Cited

Adamson, A. W., and A. P. Gast, *Physical Chemistry of Surfaces*, 104 (1997).

Asai, A., M. Shioya, S. Hirasawa, and T. Okazaki, "Impact of an Ink Drop on Paper," *J. Imaging Sci. Tech.*, **37**, 205 (1993).

Bergeron, V., D. Bonn, J. Y. Martin, and L. Vovelle, "Controlling Droplet Deposition with Polymer Additives," *Nature*, **405**, 772 (2000).

Blake, T. D., and J. De Coninck, "The Influence of Solid-Liquid Interactions on Dynamic Wetting," *Adv. Colloid Inter. Sci.*, **96**, 21 (2002).

Bussmann, M., J. Mostaghimi, and S. Chandra, "On a Three-Dimensional Volume Tracking Model of Droplet Impact," *Phys. Fluids*, **11**, 1406 (1999).

Chandra, S., and C. T. Avedisian, "On the Collision of a Droplet with a Solid Surface," *Proc. R. Soc. Lond.*, **432**, 13 (1991).

Cheng, L., "Dynamic Spreading of Drops Impacting onto a Solid Surface," *Ind. Eng. Chem. Process Des. Dev.*, **16**, 192 (1977).

de Gennes, P. G., "Wetting: Statics and Dynamics," *Rev. Mod. Phys.*, **57**, 827 (1985).

Engel, O. G., "Waterdrop Collision with Solid Surface," *J. Res. Natn. Bur. Stand.*, **54**, 281 (1955).

Ford, R. E., and C. G. L. Furmidge, "Impact and Spreading of Spray Drops on Foliar Surfaces," *Wetting. Soc. Chem. Industry Monograph*, 417 (1967).

Fukai, J., Y. Shiiba, T. Yamamoto, O. Miyataka, D. Poulikakos, C. M. Megaridis, and Z. Zhao, "Wetting Effects on the Spreading of a Liquid Droplet Colliding with a Flat Surface: Experiment and Modeling," *Phys. Fluids*, **7**, 236 (1995).

Fukai, J., M. Tanaka, and O. Miyatake, "Maximum Spreading of Liquid Droplets Colliding with Flat Surfaces," *J. Chem. Eng. Japan*, **31**, 456 (1998).

Fukai, J., Z. Zhao, D. Poulikakos, C. M. Megaridis, and Z. Zhao, "Modeling of the Deformation of a Liquid Droplet Impinging upon a Flat Surface," *Phys. Fluids*, **5**, 2588 (1993).

Harlow, F. H., and J. P. Shannon, "The Splash of a Liquid Droplet," *J. Appl. Phys.*, **38**, 3855 (1967).

Hiemenz, P. C., and R. Rajagopalan, *Principles of Colloid and Surface Chemistry*, 158 (1997).

Kim, H. Y., and J. H. Chun, "The Recoiling of Liquid Droplets Upon Collision with Solid Surfaces," *Phys. Fluids*, **13**, 643 (2001).

Lin, C. M., R. M. Ybarra, and P. Neogi, "Three- and Two-Dimensional Effects in Wetting Kinetics," *Adv. Colloid Interface Sci.*, **67**, 185 (1996).

Marmur, A., "The Radial Capillary," *J. Colloid Interface Sci.*, **124**, 301 (1988).

Mao, T., D. C. S. Kuhn, and Tran Honghi, "Spread and Rebound of Liquid Droplets upon Impact on Flat Surfaces," *AIChE J.*, **43**, 2169 (1997).

Pasandideh-Fard, M., Y. M. Qiao, S. Chandra, and J. Mostaghimi, "Capillary Effects during Droplet Impact on a Solid Surface," *Phys. Fluids*, **8**, 650 (1996).

Scheller, B., and D. W. Bousfield, "Newtonian Drop Impact with Solid Surface," *AIChE J.*, **41**, 1357 (1995).

Shaw, D. J., *Introduction to Colloid and Surface Chemistry*, 151 (1991).

Šikalo, Š., M. Marengo, C. Tropea, and E. N. Ganic, "Analysis of Impact of Droplets on Horizontal Surfaces," *Experimental Thermal and Fluid Science*, **25**, 503 (2002).

Weast, R. C., *Handbook of Chemistry and Physics*, CRC Press, pp. 6–102 (1977).

Worthington, A. M., "On the Forms Assumed by Drops of Liquids Falling Vertically on a Horizontal Plate," *Proc. R. Soc. Lond.*, **25**, 261 (1877).

Manuscript received Nov. 13, 2002, and revision received Apr. 3, 2003.